Indian Journal of Engineering & Materials Sciences
Vol. 31, June 2024, pp. 335-342
DOI: 10.56042/ijems.v31i3.8874

Growth, Characterization and Magneto-transport of single crystalline Bismuth

Naveen Kumar[a,b], Navneet Kumar Karn[a,b*], Pallavi Kushwaha[a,b] & Veerpal Singh Awana[a,b]

[a]CSIR-National Physical Laboratory, Dr. K. S. Krishnan Marg, New Delhi 110012, India

[b]Academy of Scientific and Innovative Research (AcSIR), Ghaziabad, Uttar Pradesh 201002, India

Received: 17 February 2024; Accepted: 27 April 2024

We report the growth of Bi single crystal via the modified Bridgman technique. The structural and microstructural morphological characterization of the as-grown Bismuth (*Bi)* single crystal includes Field Emission Scanning Electron Microscopy (FESEM), X-ray Diffractometer (XRD)and Energy Dispersive X-ray Analysis (EDAX). Additionally, the Raman Spectra analysis has been used to study the vibrational modes of the Bi. The UV-Vis spectroscopy has revealed a bulk band gap of approximately 5.23eV in the as-grown Bi crystal. The electrical transport measurements have demonstrated metallic behavior with an R_{300K} /R_{2K} (RRR) ratio of around 6.5. However, under the applied field, the as-grown Bi shows change from metallic to semiconducting behavior. The bulk band gap of the as-grown crystal has been indirectly determined based on its semiconducting behavior under the applied magnetic field which increases with the applied field. Notably, at low temperatures (<10K), the synthesized Bi crystal exhibits large magneto-resistance (MR) of the order of ~10^5% under applied fields up to ±14Teslaas along with Shubnikov-de Haas (SdH) oscillations.

Keywords: Crystal Growth, Topological Materials, Magneto-resistance, SdH Oscillations

1 Introduction

Bismuth (Bi) has a rhombohedral crystal structure at room temperature. It is a post-transition metal having several interesting electronic and magnetic properties. Bi and its compounds have shown potential in various applications, including in electronics, thermo-electrics, and superconductors. An interesting quantum phenomenon being exhibited by Bi, is the SdH oscillations, which is a quantum mechanical effect that occurs in the conductivity of a material when subjected to a strong magnetic field at low temperatures[1]. These oscillations are a manifestation of quantum interference effects in the motion of charge carriers, such as electrons, within the material[2-5]. These oscillations in conductivity are mostly caused by charge carriers like electrons and holes, which begin to oscillate when subjected to a strong magnetic field. Additionally, it has been noted that the primary cause of SdH oscillations is the abundance of free charge carriers present in a material's conduction band[6-8]. The application of a magnetic field to topological materials can result in unique SdH oscillations. The presence of topologically protected surface states (SS) contributes to the oscillatory behavior and the analysis of SdH oscillations in these materials provide valuable information about their electronic structure, such as the Fermi surface topology and the nature of the charge carriers[9-13]. A topological insulator is a class of quantum materials that has a unique combination of insulating behavior in the bulk of the material and metallic behavior on their surfaces[14-20]. These exceptional qualities of topological materials can demonstrate significant benefits in a range of applications, including quantum computers, thermo-electricity, magnetic sensors, spintronics, and optoelectronics[21-25]. The topological nature of systems can only be predicted by a very limited set of experimental methods. One such method is angle-resolved photoemission spectroscopy (ARPES)[26,27], however, it is a rather rigorous method for investigating topological materials due to its intricate measurements and modeling. Scientists and physicists are still fascinated by Bismuth since it has so much to offer in the field of condensed matter physics including potential applications[28-31]. Despite, ARPES, the magneto-transport measurements offer an alternate method to study the topological properties of materials.

Remarkably, contrasting findings are also reported related to the topology of Bismuth, particularly in

*Corresponding author (E-mail: nkk15ms097@gmail.com)

terms of the analysis of its magneto-transport properties; both theoretically and empirically[32-34]. To further sum up the electronic properties of as-grown Bi crystal, we have done elaborative (down to 2K and up to 14Tesla) magneto-transport experiments in the current study. This article provides a thorough overview of SdH oscillations and their dependency on magnetic fields and temperature in as-grown Bismuth.

2 Materials and Method

The Bi single crystal used in the present study is grown by the modified bridgeman method. Two grams of high-purity (99.999%) Bi is weighed and ground in an Ar gas environment inside a glove box to avoid any reaction with the atmospheric gases during the heat treatment. The well-ground powder is first pelletized with the help of a hydraulic pelletizer into a rectangular pellet and then sealed in a quartz tube under vacuum (10^{-5} Torr). A vacuum-encapsulated tube is placed in an auto-programmable furnace using optimized heat treatment profile is shown in Fig. 1, as the same reported earlier[35].

A clear image of the obtained single crystal is shown in the inset of Fig. 1, having a silvery shining surface. Using a surgical blade, thin flakes of the as-grown crystal were mechanically cleaved for further characterization. Using a Rigaku Miniflex-II X-ray diffractometer, X-ray diffraction (XRD) measurements were made on both mechanically cleaved thin flakes and finely crushed powder. Rietveld refinement was carried out with Full prof software to explore the lattice characteristics of the Bi single crystal. Energy-dispersive X-ray analysis (EDAX) measurements were carried out using Zeiss EVO-50 and field emission scanning electron microscopy (FESEM) were used to examine the surface morphology and elemental compositions. The vibrational modes present in Bismuth were studied by performing Raman spectroscopy on Renishaw in Via Reflex Raman Microscope equipped with a laser 532 nm. Further, to find out the optical band gap, UV-VIS spectroscopy measurements were performed on a UV 1800 Shimadzu spectrometer. The sample is well pulverized and dissolved homogeneously into an organic solvent before taking the UV-VIS spectrum. The Physical Property Measurement System (PPMS) from Quantum Design is used to investigate the transport properties of synthesized crystals using a traditional four-probe electrical contact geometry. The sample was mounted on a PPMS puck and Epotek H20E silver epoxy was used to make electrical connections.

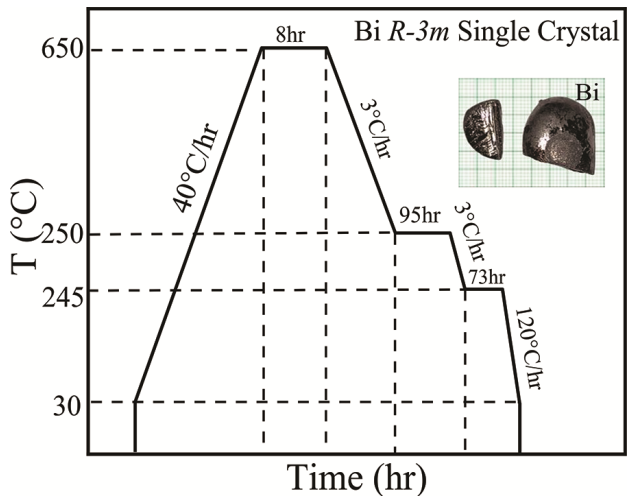

Fig. 1 — The temperature profile used for the growth of Bi single Inset shows the image of e obtained silvery shiny single crystal.

3 Results and Discussion

3.1 Crystal Characterization

3.1.1 XRD and SEM/EDAX analysis

We mechanically cleaved a thin flake from the as-grown Bi single crystal and the single crystal XRD pattern is shown in Fig. 2(a). We found layered growth along the c-axis which is revealed by the high intensity peaks having (*00l*) diffraction planes. The growth of planes is along (*003*). Also, another single crystalline domain of (202) is observed and is marked with (*) in the Figure. Interestingly, this is similar to what we found in our earlier preliminary study on magneto–transport of modified bridgeman based Bi crystal[35]. Further, we performed XRD measurement on the finely crushed powder to accomplish its phase purity in range from 10º to 80º at ambient conditions. To estimate the lattice parameters and various co-ordinate positions, the Rietveld analysis is done for the observed PXRD and the results are shown in Fig. 2(b). Both observed and refined patterns match well with each other. The Rietveld analysis unfolded that the as-grown crystals belong to the $R\bar{3}m$ space group with the rhombohedral crystal structure. The calculated lattice parameters, along with the co-ordinate positions as obtained from Rietveld refinement are displayed in Table 1. The unit cell structure is created using VESTA software using the CIF (Crystallographic Information File) produced

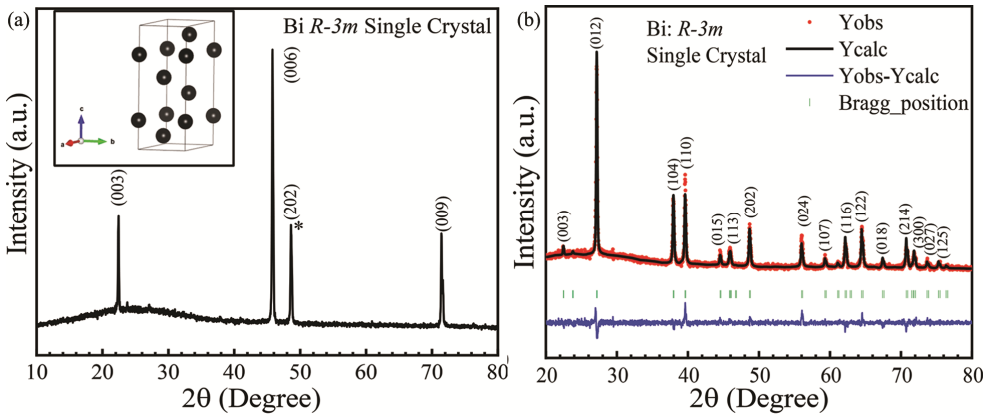

Fig. 2 — (a) XRD pattern taken on mechanically cleaved single crystal flake of synthesized Bi crystal. The inset shows the unit cell structure of the synthesized Bi single crystal processed in VESTA software, and (b) Rietveld refined powder XRD spectra taken on finely ground as-grown Bi single crystal.

Table 1 — Bi single crystal Parameters obtained from Rietveld Refinement

Cell Parameters	Refinement parameters
Cell Type: Rhombohedral	χ^2=1.53
Space Group: R$\bar{3}$m	R_p=6.20
Lattice Parameters:	R_{wp}=7.93
a=b=4.549Å & c=11.866Å	R_{exp}=6.40
α=β=90°&γ=120°	
Cell Volume:	212.645 Å^3
Density:	19.584g/cm^3
Atomic coordinates:	Bi1 (2/3, 1/3, 0.098)
	Bi2 (1/3, 1/3, 0.902)

by the Rietveld refinement and is displayed in the inset of Fig 2(a). Figure 3(a) shows the obtained EDAX spectra and the inset table shows that no other impurity has been observed. The single crystalline nature is Bi has been confirmed by the layered type of growth as clearly visible in the FESEM image (inset of Fig. 3(a)).

3.1.2 Raman and UV-VIS spectroscopy

The studied Bi crystal observed Raman modes being recorded at ambient temperature are shown in Fig. 3(b). The two peaks observed are Lorentz de-convoluted and fitted. The two identified peaks are found at 69±1 and 95±1 cm^{-1}, corresponding to the vibrational modes of E_g and A_{1g}. The schematics of the vibrational modes of the Bismuth atom are shown in the inset of Fig. 3(b). The measured peaks match well with earlier findings[35-37].

Figure 3(c) shows the UV-VIS spectrum of the as-synthesized Bi single crystal. Primarily, the basic absorption spectra are the result of electron excitation to the conduction band from the valance band. The clear and unique deviation is used to figure out the optical band gap measurement of the synthesized Bi single crystal. The calculated optical band gap is around 5.23eV, which is comparable to the band gap being seen at X high symmetry point in the DFT calculated band structure of Bi[38]. Interestingly, though the observed bulk band gap is close to highly semi-metallic or insulating regime, albeit the studied Bi crystal is highly metallic due to its topological character. We discuss this in later sections.

3.2 Transport measurements

3.2.1 Electronic transport

Figure 4(a) shows the R-T plot, which suggests metallic behavior for the synthesized Bi single crystal and the inset image shows the experimental schematics of the transport measurements. In metallic materials, electrical resistance generally decreases with decreasing temperature, and this behavior is often characterized by a downward slope on the R-T plot. The temperature range of the plot is from 300K (room temperature) to 2K (very low temperature). The Residual Resistance Ratio (RRR) is defined as the ratio of the electrical resistance at room temperature to the resistance at the lowest measured temperature. In this instance, the obtained RRR value, which is the ratio of the resistance at 300K to the resistance at 2K (R_{300K}/R_{2K}), is 6.5. A high RRR value indicates a large decrease in the electrical resistance from room temperature to the low temperature range, which is a characteristic feature of high-quality metallic conductors[39].

3.2.2 Magneto-transport

Figure 4(b) illustrates how the resistance of the Bi single crystal changes with temperature at different applied magnetic fields. The resistance of the Bi

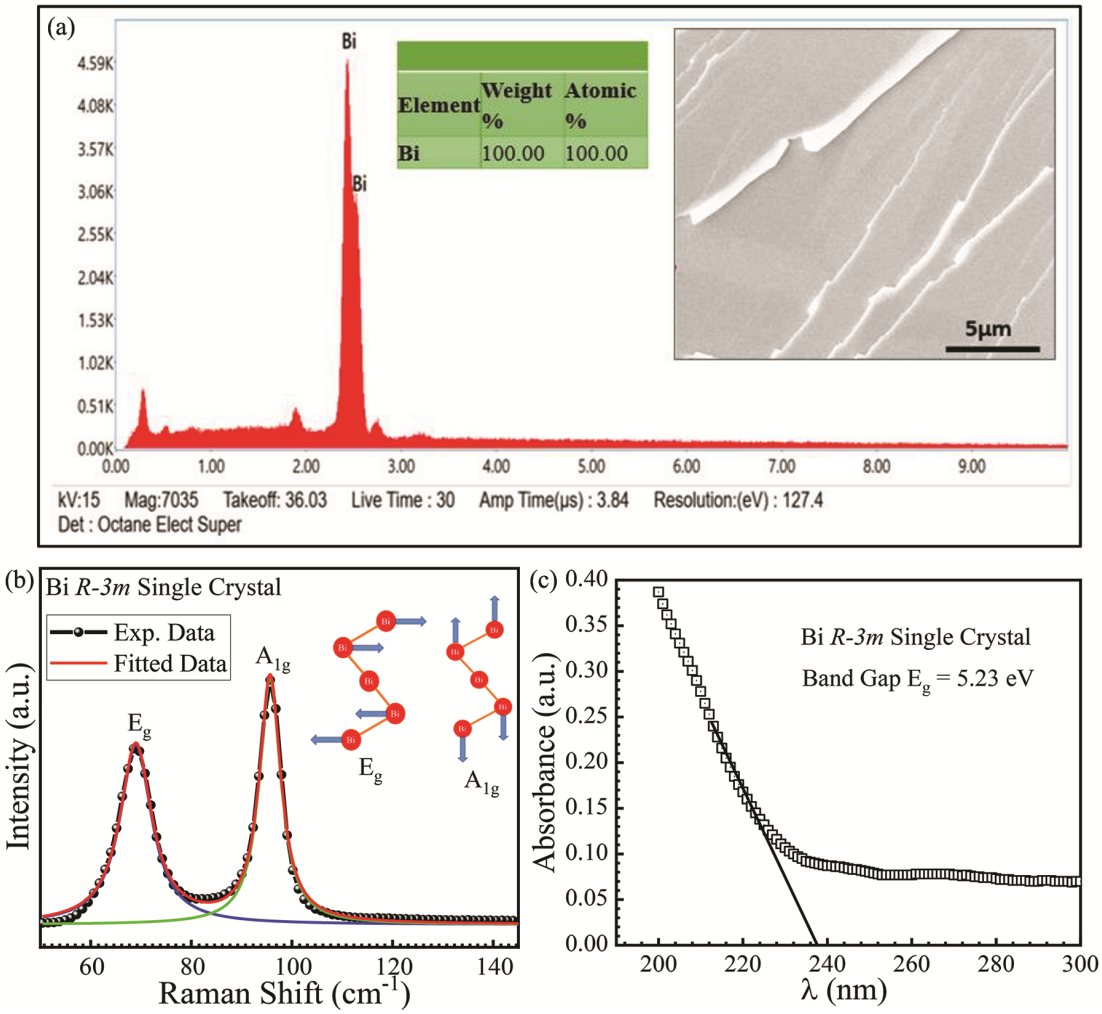

Fig. 3 — (a) EDAX spectra of synthesized Bi single crystal, in which the inset table displays the elemental composition of constituent elements and the inset is FESEM image shows surface morphology of synthesized Bi single crystal, (b) Lorentz deconvoluted Raman spectrum of Bi single crystal at room temperature and the inset shows the schematic vibrational modes of Bi atoms, and (c) The UV-VIS spectroscopy of as-synthesized Bi crystal.

single crystal increases continuously over a wide temperature range (2 to 300 K) when subjected to magnetic fields of 2, 4, 6, 8, 10, 12, and 14Tesla.This suggests that the magnetic field has a notable effect on the electrical properties of the crystal. The semiconducting behavior of Bismuth emerges in the presence of transverse fields, see inset Fig. 4(a). At zero field, Bismuth shows metallic behavior as shown in the R-T plot. The band gap of a semiconductor follows the relation $R(T) \propto exp(E_g/k_BT)$, where E_g is band gap and $k_B$is Boltzmann constant. Using this relation, the band gap induced by the applied magnetic field is calculated. Figure 4(c) shows the ln(R) vs. 1/T plot. The slope is determined by fitting a straight line and thus obtaining the band gap. The inset of

Fig. 4(c) shows the variation of the band gap with the applied field. The square root dependence of the band gap is illustrated through the fitted curve. These results affirm the theoretical predictions of the two-band model of *k.p* theory for bismuth by Smith *et al.*[40], exhibiting square root dependence on the applied transverse magnetic field. Further, features present in magneto-transport are extracted by calculating the temperature derivative of resistance at different applied fields which is shown in Fig. 4(d). The temperature derivative becomes more negative as we go down to temperature T_1.This shows above temperature T_1 being marked in the figure, the semiconducting region is more prominent above T_1. The characteristic temperature T_1 shifts to a higher temperature for higher transverse fields. For 2Tesla,

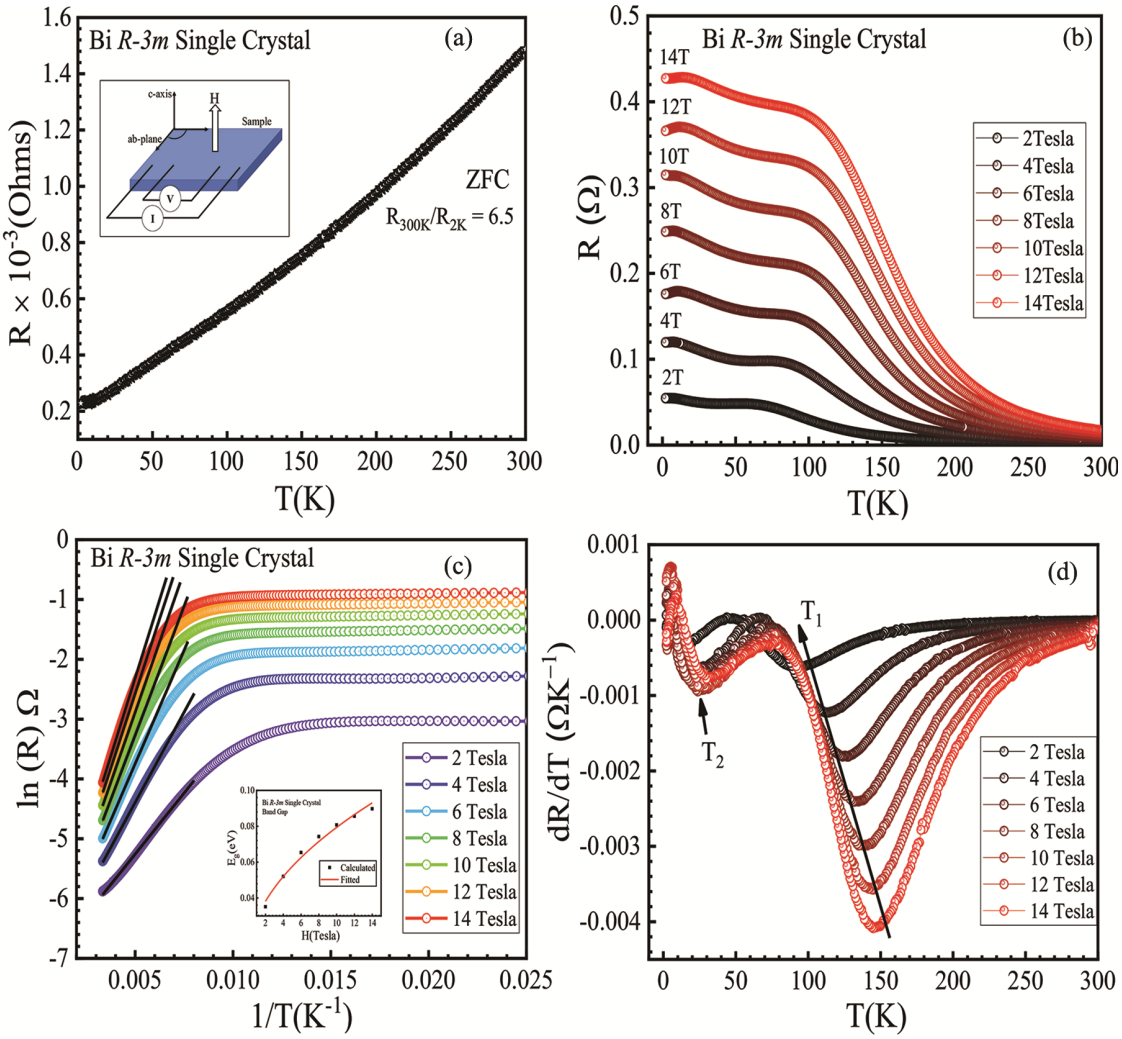

Fig. 4 — (a) Variation in the electrical resistivity as a function of temperature from 300-2K. The inset depicts experimental schematics for magneto-transport measurements, (b) Temperature dependence of electrical resistance measured at different transverse magnetic fields, (c) Natural logarithm of resistance showing band gap due to applied magnetic field. The inset maps the variation in the experimental band gap against the applied magnetic field. (d) The first-order temperature derivative of resistance at different applied transverse magnetic fields.

T_1 is ~92K, which shifts to ~145K at 14Tesla. In Fig. 4(b), below the semiconducting region (< T_1), two humps are observed. The second minima in dR/dT marks the second hump in the field-dependent RT plot and is marked by T_2 in Fig. 4(d). Below 10 K, the slope dR/dT becomes positive implying a decrease in resistance which shows a deviation from the semiconducting behavior below 10K. Notably, the SdH oscillations are also observed below 10K, which we discuss later. In previous studies of Bismuth[41], single humps are observed in RT measurement under transverse fields. As per our knowledge, for the first time, two characteristic humps are observed in Bismuth. At low temperatures, Bismuth shows peculiar characteristics, which need further investigation. Interestingly, Bismuth is reported to have superconducting properties as well at very low temperatures (~mK)[42].

3.2.3 Magnetoresistance

To investigate the topological properties of as-grown Bi single crystal, magneto-transport measurements were performed for the applied transverse field in the range 0-14Tesla. Figure 5(a) represents the MR% vs H plot for the applied transverse field up to 14Tesla at various temperatures. The MR %is calculated using the formula; $MR\% = \left[\frac{R(H)-R(0)}{R(0)}\right] \times 100$, where R(H) is the resistance at applied field(H)and R(0) is the resistance in the

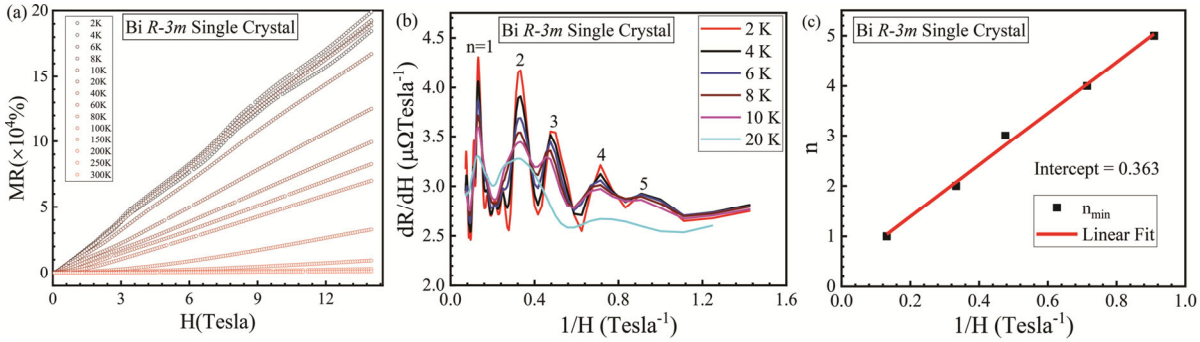

Fig. 5 — (a) MR% vs. applied magnetic field up to +14T at different temperatures and the inset shows an enlarged view of MR% at low fields exhibiting LMR at low temperatures (<10K), and (b) The behavior of dR/dH of Bi crystal as a function of the inverse magnetic field at different temperatures (c) Linearly fitted Landau level fan diagram for temperature 2K

absence of any field.The Bi single crystal shows a non-saturating, very high MR% ~1.8 ×10^5% in the field range of 0-14Tesla at 2K. As the temperature increases, the MR% tends to decrease in the same range of applied field, for example, MR% is found to be ~ 1000% at 300K. For the conventional metallic systems, the MR shows a quadratic dependency on the applied field as predicted by classical theory. For Bi single crystal, the observed MR% shows linear dependency on the applied transverse magnetic field at low temperatures (<10K). At higher temperatures, the MR% vs. H plot has the parabolic shape showing classical behavior. In contrast to the classical transport, the linear MR (LMR) indicates a different transport mechanism involved in the Bi single crystal. The non-saturating LMR may originate due to Quantum effects[43], which can be observed (i) in a polycrystalline sample due to the averaging effect[44] (ii) in a heavily disordered system[45](iii) in topological materials with Dirac electrons[46]. The high-field LMR can be interpreted by the quantum limit of Landau Levels (LL) in high fields[43,44]. The LMR at low fields is the characteristic feature of topological Dirac electrons[46]. The Bi single crystal exhibits LMR at high as well as low fields. Since as-grown Bi single crystal does not fall into the category (i) or (ii), the low field LMR at low temperature [see inset Fig.5(a)] indicates the presence of Dirac electrons in Bismuth, whereas the quantum limit of the LL can explain the LMR at higher fields. The LLs are key to understanding the quantum oscillation exhibited in 2D electrons. In the context of Bismuth, the same is discussed below.

3.2.4 SdH Oscillations

The single crystal of Bi is well known for its quantum oscillations at low temperatures[1,35]. To retrieve these oscillations in as-synthesized Bi single crystal, at different temperatures, the first order derivative of resistance with respect to the applied field is calculated and plotted against the inverse of the applied magnetic field as shown in Fig. 5(b). The oscillating behavior of dR/dH shows the periodic change of peaks against the inverse magnetic field due to the SdH effect. Furthermore, the dependency of maxima/minima placements on transverse magnetic fields raises the possibility that 2D surface states are the source of SdH oscillations. The cross-section area of the Fermi surface is dependent on the frequency of quantum oscillations in the transverse magnetic field, which indicates the existence of the surface.

To examine the topological nature of Bi as primarily indicated by MR data analysis, the Berry phase is calculated from the quantum oscillation data using the Landau level (LL) fan diagram. As seen in Fig. 5(c), the Landau index (n) is represented as a function of the inverse magnetic field in the LL fan diagram. At low temperature, as indicated by the plateau region, charge carrier behave as quasi 2D gas. In the presence of magnetic field quasi 2D gas forms Landau Levels. The Landau levels split and get separated as the field is increased. The nth index at magnetic field H implies that the conduction of charge carriers is through the n^{th} Landau Level. At a given field H, the n^{th} Landau Level is crossing the Fermi Level. Here, the LL index is increased by 1 between neighboring maxima. The integral LL index has been assigned to a maxima of quantum oscillations in the dR/dH versus 1/H plot following n→ 0 in the infinite transverse field limit. Using the Lifshitz-Onsager quantization rule, the LL index *n* is found inversely proportional to the applied magnetic field, which can be expressed as $A_F\hbar/eH = 2\pi(n + \beta)$; here, $2\pi\beta$ is the Berry's phase and $A_F$is the cross-section area of the Fermi surface. In the LL fan diagram, linear fitting of data points is represented

using the solid line and the linear extrapolation of this line yields a finite intercept of 0.363, resulting to a Berry's phase of 0.726π. The Berry's phase value is non-zero, which gives indication of the topological nature of SdH oscillations coming from the surface states and agrees with the literature on various topological insulators. The slope of the LL fan diagram for SdH oscillations is given as $n_{2D}h/2e$[47,48], where n_{2D} is the 2D charge carrier density. From the linear fitting of Fig. 5 (c), the surface charge carrier density is determined to be $n_{2D} \approx 2.5\times10^{17}$m^{-2} which is comparable and in accordance with the previous reports[35,49]. By using the formula $n_{2D} = k_F^2/4\pi$,the Fermi wave vector k_F can be calculated and is found to be 0.177 Å^{-1}.Further, assuming a circular cross-section of the Fermi surface, the Fermi surface's cross-sectional area A_F is calculated using the expression $k_F = (A_F/\pi)^{1/2}$, which is 9.97×10^{17}m^{-2}. The SdH oscillation frequency (F) is related to the Fermi surface's cross-section area (A_F) via relation $F = (\hbar/2\pi e)A_F$, according to the Onsager relation. Here, e and $\hbar$ are the electronic charge and Plank's constant, respectively. From the above relation, the SdH oscillation frequency calculated is 10.4Tesla.

4 Conclusion

Summarily, in the present study, *Bi* single crystals of were synthesized using solid-state reaction method. The crystal's phase purity, chemical composition and morphology have been thoroughly characterized. The R-T measurements reproduce the well-known metallic behavior of topological rhombohedral Bismuth. Under the applied field, RT measurements of as-grown Bismuth exhibit semiconducting behavior. Remarkably, at low temperatures, the synthesized Bi exhibits a huge magneto-resistance (MR%) ~ 10^5 order under an applied field of up to +14Tesla. The LMR at low temperatures and low fields indicates the presence of topological states. Further, RH data at low temperatures (up to 10K) exhibit the known SdH oscillations which are analyzed by calculating the LL fan diagram. The SdH indicated the presence of a single pocket close to the Fermi surface with a characteristic single frequency peak at around 10.4Tesla, which is the conclusion of the present study on as grown rhombohedral Bismuth.

Acknowledgement

The authors are thankful to the Director of the National Physical Laboratory for his encouragement and keen interest in research activities. The authors would like to acknowledge Dr. J. S. Tawale for FESEM measurements and Mrs. Shaveta Sharma Sharda for Raman spectroscopy. Naveen Kumar is thankful to CSIR, India for the research fellowship and to AcSIR, India for Ph.D. registration. This research is funded by in-house project no. OLP240832 and OLP240232.

References

1 Lerner L S, *Phys Rev*, 127 (1962) 1480.
2 Taskin A A& Ando Y, *Phys Rev B*, 80 (2009) 085303.
3 Zhang L, Song X Y & Wang F, *Phys Rev Lett*, 116 (2016) 046404.
4 Zhao W, Chen L, Yue Z, Li Z, Cortie D, Fuhrer M & Wang X, *npj Quantum Mater*, 4 (2019) 56.
5 Shrestha K, Marinova V, Graf D, Lorenz B & Chu C W, *Phys Rev B*, 95 (2017) 075102.
6 Sasmal S, Saini V, Bruyant N, Mondal R, Kulkarni R, Singh B, Tripathi V &Thamizhavel A, *Phys Rev B*, 104 (2021) 205135.
7 Zhang L, Helm T, Lin H, Fan F, Le C, Sun Y, Markou A & Felser C, *Adv Mater*, 33 (2021) 2102107.
8 Zhao L, Xu L, Ding L, Zuo H & Zhu Z, *Phys Rev B*, 102 (2020) 075139.
9 Alexandradinata A, Wang C, Duan W & Glazman L, *Phys Rev X*, 8 (2018) 011027.
10 Bardarson J H & Moore J E, *Rep Prog Phys*, 76 (2013) 056501.
11 Ren Z, Taskin A A, Sasaki S, Segawa K & Ando Y, *Phys Rev B*,85 (2012) 155301.
12 Tian M, Ning W, Qu Z, Du H, Wang J & Zhang Y, *Scientific Reports*, 3 (2013) 1212.
13 Niu W, Du K, Wang S, Zhang M, Gao M, Chen Y, Liu H, Zhou W, Song F, Wang P & Xu Y, *Nanoscale*, 9 (2017) 12372.
14 Hu J, Xu S Y, Ni N & Mao Z, *Annu Rev Mater Res*, 49 (2019) 207.
15 Sbierski B, Pohl G, Bergholtz E J and Brouwer P W, *Phys Rev Lett*, 113 (2014)026602.
16 Yang M X, Luo W & Chen W, *Adv Phys X*, **7** (2022) 2065216.
17 Kane C L, in *Contemporary Concept ofCondensed Matter Science*,Vol IV, edited by Franz M& Molenkamp L (Elsevier)(2013) 3.
18 Gao H, Venderbos J W, Kim Y & Rappe A M, *Annu Rev Mater Res*, 49 (2019)153.
19 Schnyder A P, Ryu S, Furusaki A & Ludwig A W, *Phys Rev B*, 78 (2008) 195125.
20 Culcer D, *Physica E: Low-Dimensional Systems and Nanostructures*, 44 (2012) 860**.**
21 Luo C W, Wang H J, Ku S A, Chen H J, Yeh T T, Lin J Y, Wu K H, Juang J Y, Young B L, Kobayashi T & Cheng C M, *Nano Letters*, 13 (2013) 5797.
22 Giustino F, Lee J H, Trier F, Bibes M, Winter SM, Valentí R, Son Y W, Taillefer L, Heil C, Figueroa A I &Plaçais B, *J Phys Mater*, 3 (2021) 042006.
23 Sánchez-Barriga J, Battiato M, Krivenkov M, Golias E, Varykhalov A, Romualdi A, Yashina LV, Minár J, Kornilov O, Ebert H & Held K, *Phys Rev B*, 95 (2017) 125405.

24 Kumar N, Ruzicka BA, Butch NP, Syers P, Kirshenbaum K, Paglione J & Zhao H, *Phys Rev B*, 83 (2011) 235306.
25 McIver JW, Hsieh D, Drapcho SG, Torchinsky DH, Gardner DR, Lee YS & Gedik N, *Phys Rev B*, 86 (2012) 035327.
26 Zhang C, Li Y, Pei D, Liu Z & Chen Y, *Annu Rev Mater Res*, 50 (2020) 131.
27 Lv B, Qian T & Ding H, *Nat Rev Phys*, 1 (2019) 609.
28 Ito S, Feng BJ, Arita M, Takayama A, Liu RY, Someya T, Chen WC, Iimori T, Namatame H, Taniguchi M & Cheng CM, *Phys Rev Lett*, 117 (2016) 236402.
29 Schindler F, Wang Z, Vergniory MG, Cook AM, Murani A, Sengupta S, Kasumov AY, Deblock R, Jeon S, Drozdov I &Bouchiat H, *Nat Phys*, 14 (2018) 918.
30 Nayak A K, Reiner J, Queiroz R, Fu H, Shekhar C, Yan B, Felser C, Avraham N & Beidenkopf H, *Sci Adv*, 5 (2019) 6996.
31 Ning W, Kong F, Hu J, Han Y, Yang J, Du H, Zhang Y and Tian M, *Appl Phys Lett*, 110 (2017)123101.
32 Yao M Y, Zhu F, Han C Q, Guan D D, Liu C, Qian D & Jia J F, *Sci Rep*, 6 (2016) 21326.
33 Kang W, Spathelf F, Fauqué B, Fuseya Y and Behnia K, *Nat Commun*, 13 (2022) 189.
34 Ohtsubo Y & Kimura S I, *New J Phys*, 18 (2016) 123015.
35 Kumar Y, Sharma P, Karn N K & Awana V P S, *J Supercond Nov Magn*, 6 (2023) 389.
36 Trentelman K, *J. Raman Spectrosc*, 40 (2009) 585.
37 Zepeda M A, Picquart M & Haro-Poniatowski E, *MRS Online Proceedings Library*, 1477 (2012) 28.
38 Fuseya Y, *J Phys Conf Ser*, 603 (2015) 012003.
39 Fors R, Khartsev S I & Grishin A M, *Phys Rev B*, 71 (2005) 045305.
40 Smith G E, Baraff G A & Rowell J M, *Phys Rev*, 135 (1964) A1118.
41 Zabila Y, Marszalek M, Krupinski M, Zarzycki A & Perzanowski M, *Coatings*, 11 (2021) 175.
42 Prakash O, Kumar A, Thamizhavel A & Ramakrishnan S, *Science,* 355 (2017) 52.
43 Abrikosov A A, *Phys Rev B*, 58 (1998) 2788.
44 Abrikosov A A, *EPL*, 49 (2000) 789.
45 Parish M M& Littlewood P B, *Nature*, 426 (2003) 162.
46 Sun Y, Taen T, Yamada T, Pyon S, Nishizaki T, Shi Z and Tamegai T, *Phys Rev B*, 89 (2014) 144512.
47 Cao H, Tian J, Miotkowski I, Shen T, Hu J, Qiao S & Chen Y P, *Phys Rev Lett*, 108 (2012) 216803.
48 Paulino R T & Avila M A, arXiv: 2306.00827 (2023).
49 Pan Y, Nikitin A M, Wu D, Huang Y K, Puri A, Wiedmann S, Zeitler U, Frantzeskakis E, Van Heumen E, Golden M S & De Visser A, *Solid State Commun,* 227 (2016) 13.